Supporting Information

Anchoring IrPdAu Nanoparticles on NH_2-SBA-15 for Fast Hydrogen Production from Formic Acid at Room Temperature

*Yixing Luo, Qifeng Yang, Wendan Nie, Qilu Yao, Zhujun Zhang, Zhang-Hui Lu**

Institute of Advanced Materials (IAM), College of Chemistry and Chemical Engineering, Jiangxi Normal University, Nanchang, 330022, China.

E-mail: luzh@jxnu.edu.cn

Table of Contents

Experimental Section

Synthesis of Mesoporous Silica (SBA-15). SBA-15 was synthesized using Pluronic® 123 as templating agent under classical acidic conditions, as previously reported by Zhao et al [S1]. Briefly, 4.0 g Pluronic® 123 was completely dissolved in 94 mL water, followed by addition of 20 mL concentrated HCl. After that, 8.8 g TEOS was added dropwise within 30 min and stirred at 313 K for 24 h. The white gel was thereafter transferred into a Teflon-lined autoclave for hydrothermal treatment at 373 K for 24 h. The obtained solid was separated by filtration, washed with sufficient amount of distilled water until neutral pH and dried at 333 K overnight. Before use, the material was calcined at 823 K for 6 h to produce the template-free mesoporous silica. The calcined sample was hereafter denoted as SBA-15.

Synthesis of Amine-modified Mesoporous SiO_2 (NH_2-SBA-15). Modification of SBA-15 with amine groups was carried out under conventional anhydrous grafting conditions referring to a reported procedure with minor modifications [S2]. Typically, 1 g SBA-15 was treated at 378 K overnight before dispersed in 60 mL toluene. Then, 6 mL of APTES was added into the mixture under vigorously stirring. Above suspension solution was refluxed at 353 K for 24 h under nitrogen atmosphere. After cooled to room temperature, the solid was then separated from the solution by centrifugation, washed with ethanol for three times, and dried at 313 K under vacuum overnight. Finally, NH_2-SBA-15 was obtained as a white powder. In addition, to obtain varying amine groups loading on SBA-15, varying dosage of APTES (0, 1.5 mL, 3.0 mL, and 9.0 mL) was added.

Synthesis of IrPdAu/SBA-15. The preparation of IrPdAu/SBA-15 was conducted according to the same procedure as IrPdAu/NH_2-SBA-15 expect that the catalyst supports is SBA-15 without amine groups.

Characterization of catalysts. X-ray diffraction (XRD) patterns were collected on Rigaku Rint-2200 X-ray diffractometer with Cu Kα radiation. Scanning electron microscope (SEM, SU 8020) and transmission electron microscopy (TEM, JEM-2100) were taken to investigate the microstructure of the as-prepared catalysts. High-angle annular dark-field scanning TEM (HAADF-STEM) and elemental

mappings were collected on JEOL JEM-ARM200F at an accelerating voltage of 200 KV. Nitrogen adsorption-desorption isotherms were measured on the Micromeritics ASAP 2460 instrument at 77 K. Inductively coupled plasma-optical emission spectrometry (ICP-OES) was recorded on an Agilent 720ES. Elemental analyses (N, C, and H) were carried out with a Euro Vector EA 3000 Analyser. The gas production from FA was detected by gas chromatograph (Fuli, GC9790) with thermal conductivity detector (TCD) and flame ionization detector (FID)-Methanator. X-ray photoelectron spectroscopy (XPS) analyses were operated on a Thermo ESCALAB 250Xi X-ray photoelectron spectrometer with an Al Kα source.

Calculation methods

$$\chi_a = \frac{P_{atm}V_{gas}/RT}{2n_{FA}} \qquad (1)$$

Where χ_a is conversion of FA, P_{atm} is atmospheric pressure, V_{gas} is volume of produced gas (H_2+CO_2), R is universal gas constant, T is room temperature (298 K), and n_{FA} is mole number of FA.

$$TOF_{initial} = \frac{P_{atm}V_{gas}/RT}{2n_{metal}t} \qquad (2)$$

Where $TOF_{initial}$ represents the initial turnover frequency when χ_a reaches 20%, n_{metal} is total mole number of metal in catalyst, and t is reaction time when χ_a reaches 20%.

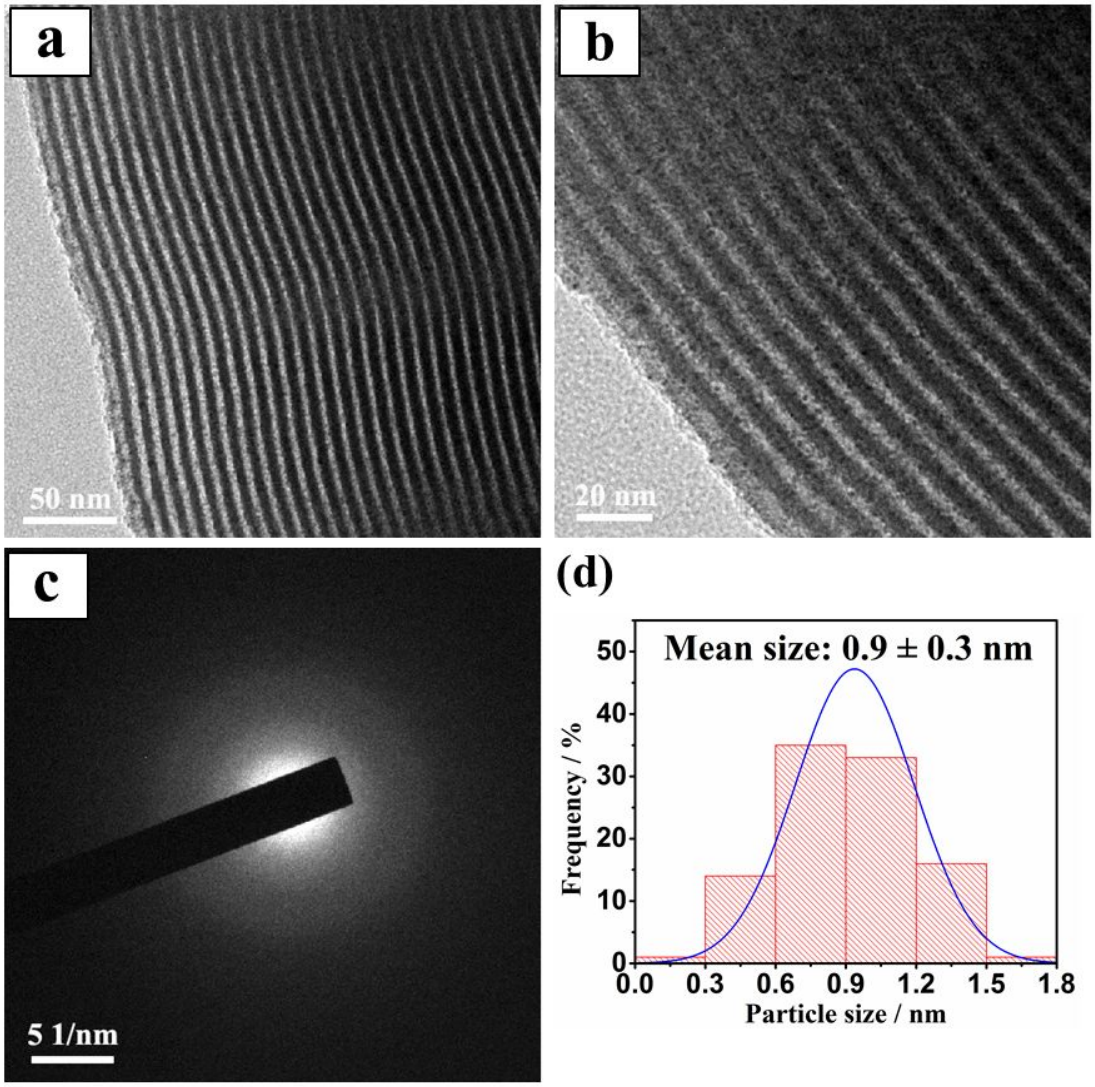

Figure S1. (a,b) TEM images, (c) SAED pattern, and (d) particle size distribution of Ir/NH_2-SBA-15.

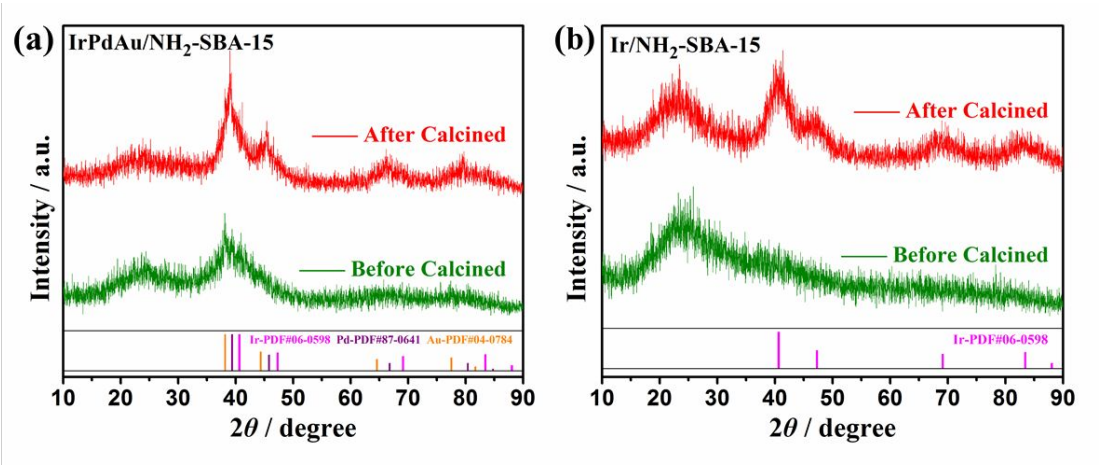

Figure S2. Wide-angle XRD patterns of (a) IrPdAu/NH_2-SBA-15 and (b) Ir/NH_2-SBA-15 before/after calcined at 873 K for 4 h under Ar atmosphere.

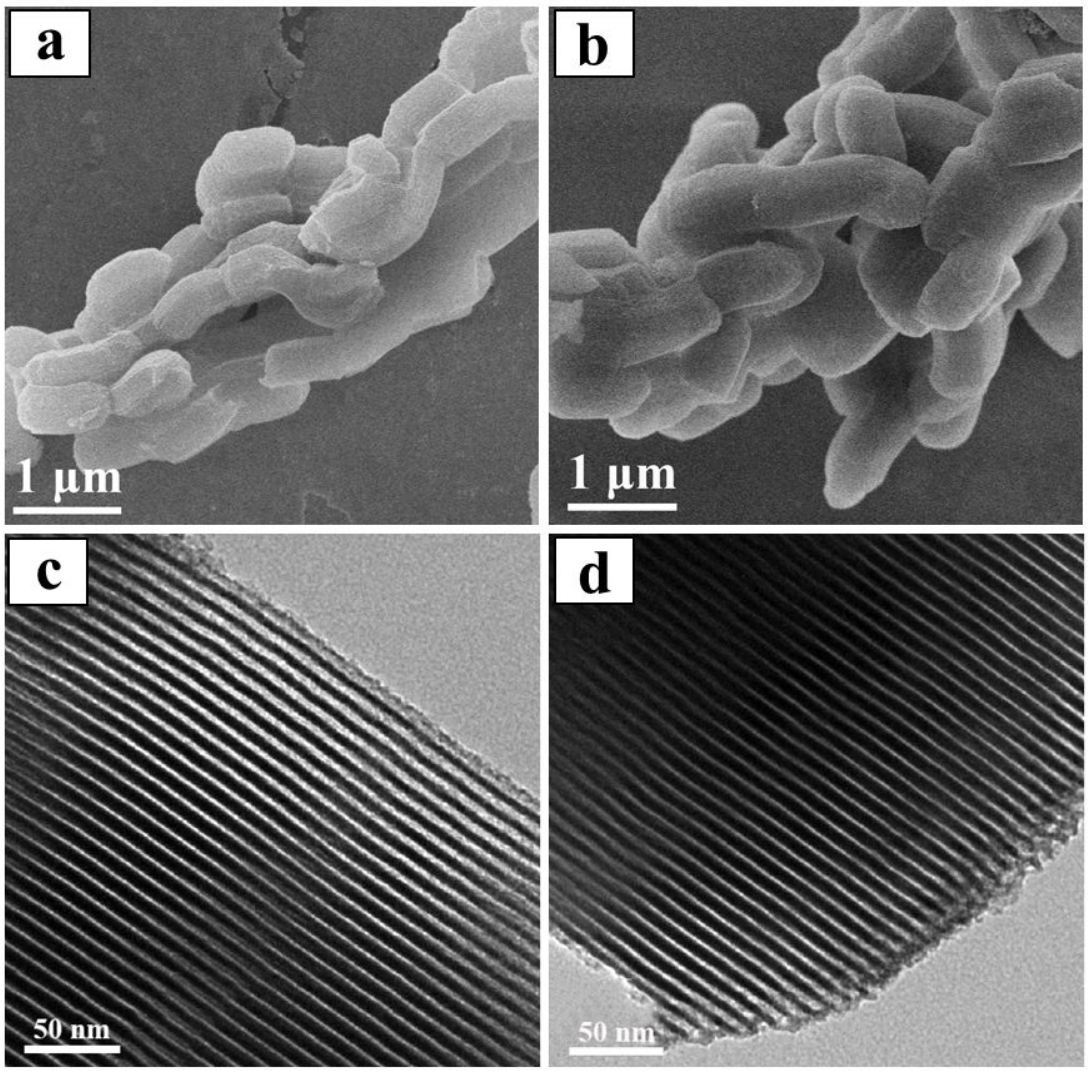

Figure S3. SEM and TEM images of (a,c) SBA-15 and (b,d) NH_2-SBA-15.

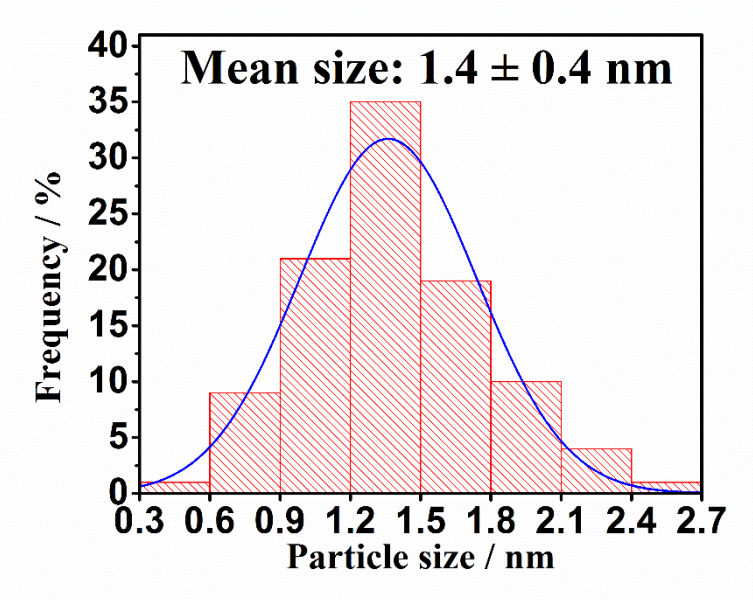

Figure S4. Particle size distribution of IrPdAu/NH_2-SBA-15.

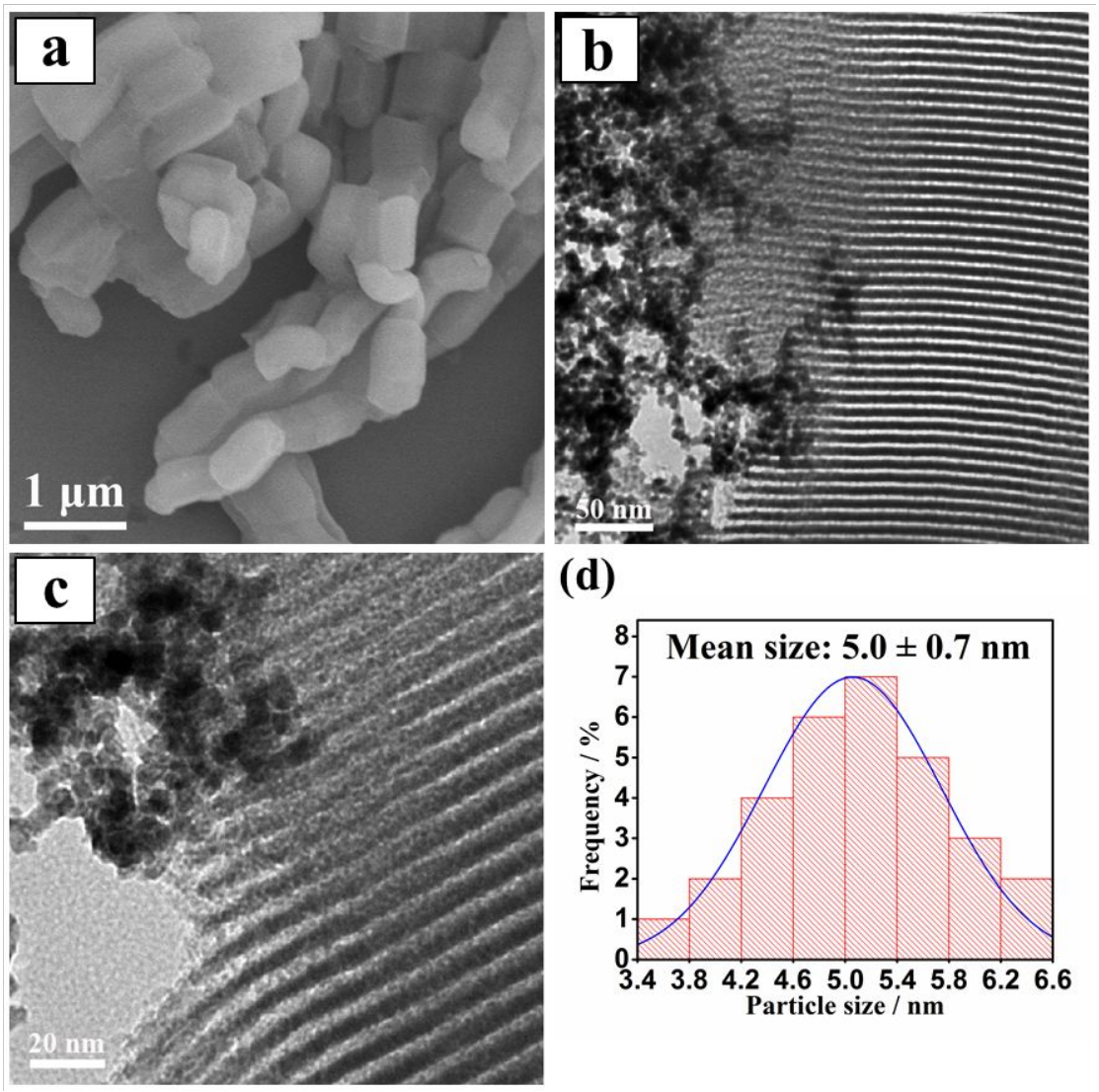

Figure S5. (a) SEM image, (b,c) TEM images, and (d) corresponding IrPdAu particle size distribution of IrPdAu/SBA-15.

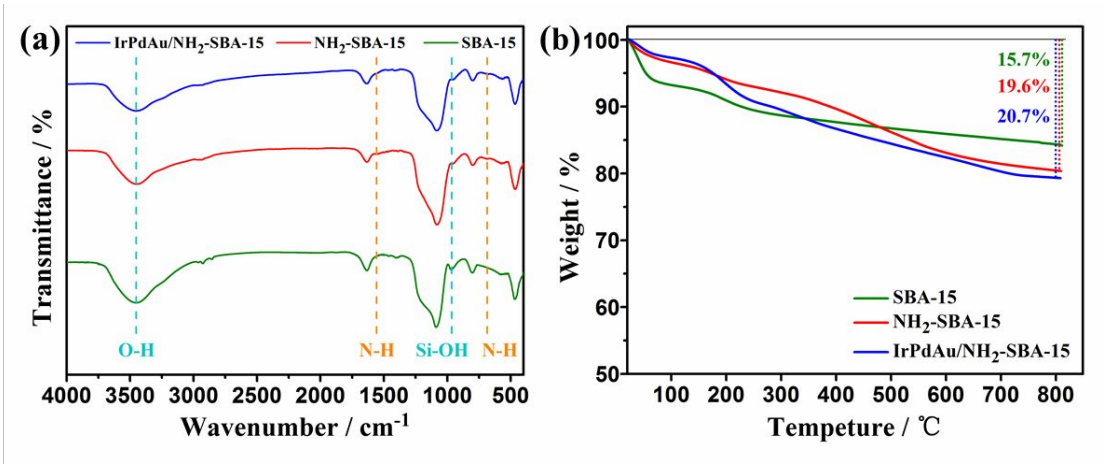

Figure S6. (a) FT-IR spectrum and (b) TGA curves of SBA-15, NH_2-SBA-15, and IrPdAu/NH_2-SBA-15.

As shown in Figure S6a, new peaks at 1554 cm^{-1} and 686 cm^{-1} appeared after APTES modification, which was ascribed to N-H as δ vibration and γ vibration in amine groups, respectively [S3-S5]. Furthermore, the intensity of the characteristic band of the Si-OH stretching mode centered at 960 cm^{-1} in amine-modified SBA-15 decreased as compared to that in SBA-15, suggesting that the surface silanol groups were replaced with APTES [S5-S7]. Further analysis of the amine-modified SBA-15 was performed using TGA and the results are shown in Figure S6b. All samples present the slight weight loss at below 200 ℃ and significant weight loss at 200-800 ℃. The former weight loss is due to the desorption of physisorbed water and the weight loss at 200-800 ℃ can be ascribed to the decomposition of grafted silane and dehydroxylation of residual silanol groups on SBA-15 [S4,S7].

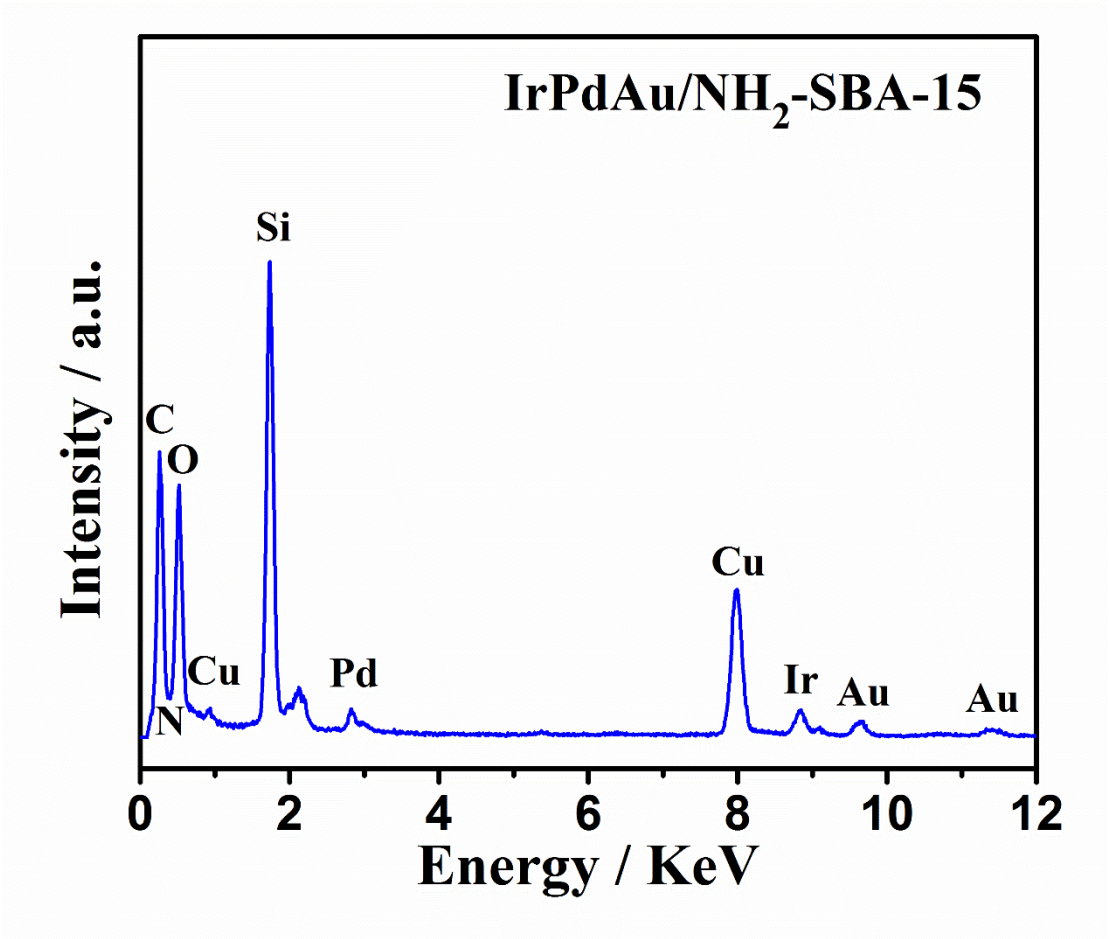

Figure S7. EDS spectrum of IrPdAu/NH_2-SBA-15.

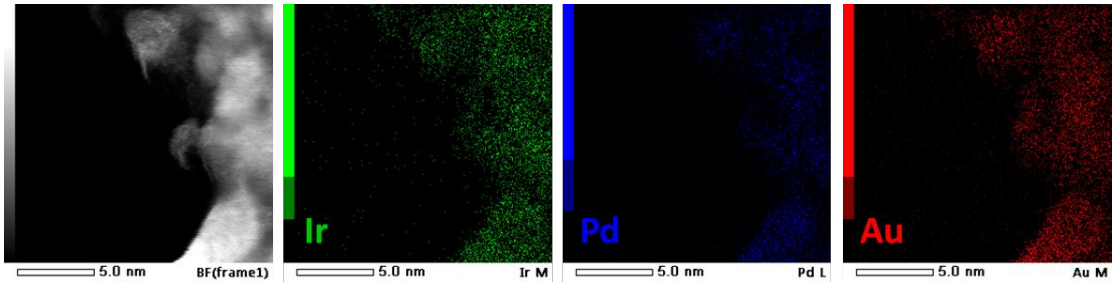

Figure S8. EDS microscale elemental mappings of IrPdAu alloy NPs supported by NH_2-SBA-15.

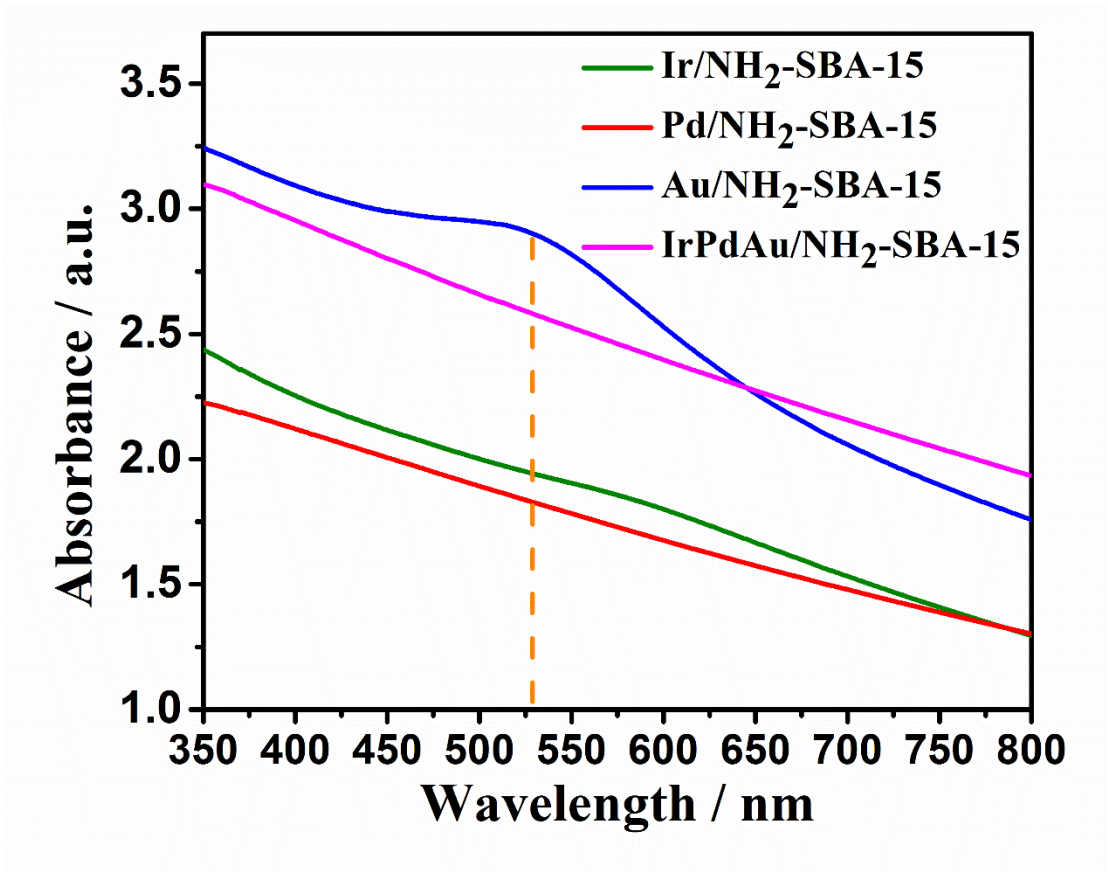

Figure S9. UV-Vis spectrum of Ir/NH_2-SBA-15, Pd/NH_2-SBA-15, Au/NH_2-SBA-15, and IrPdAu/NH_2-SBA-15.

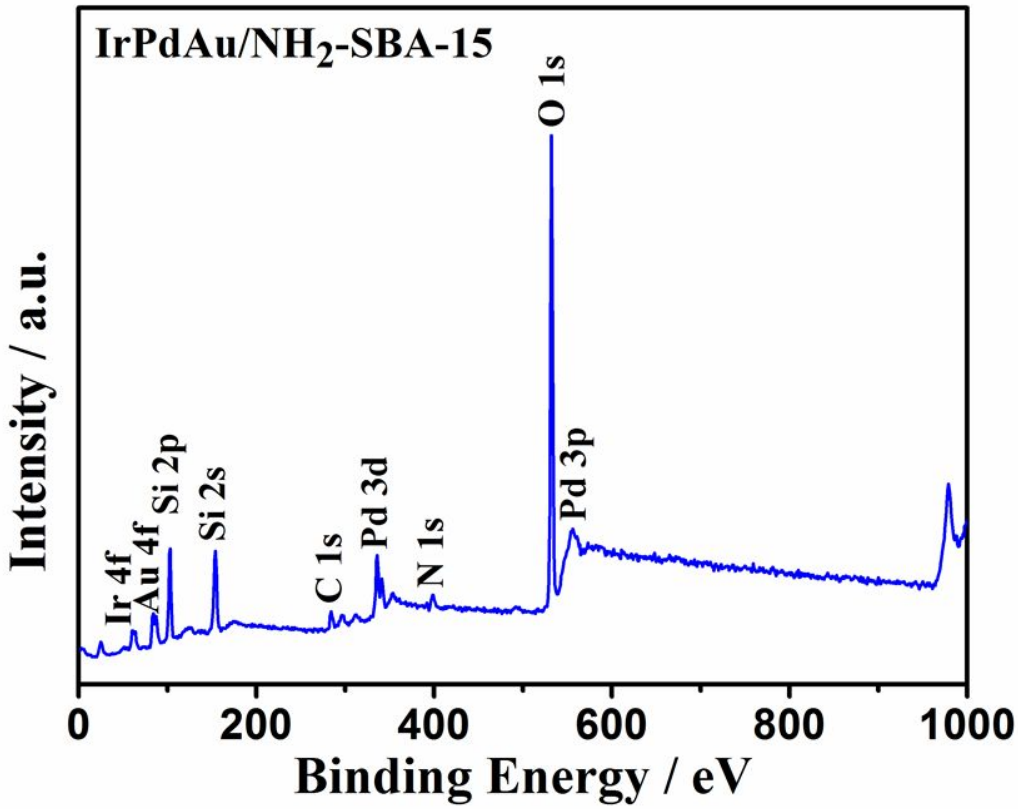

Figure S10. The survey XPS spectrum of IrPdAu/NH_2-SBA-15.

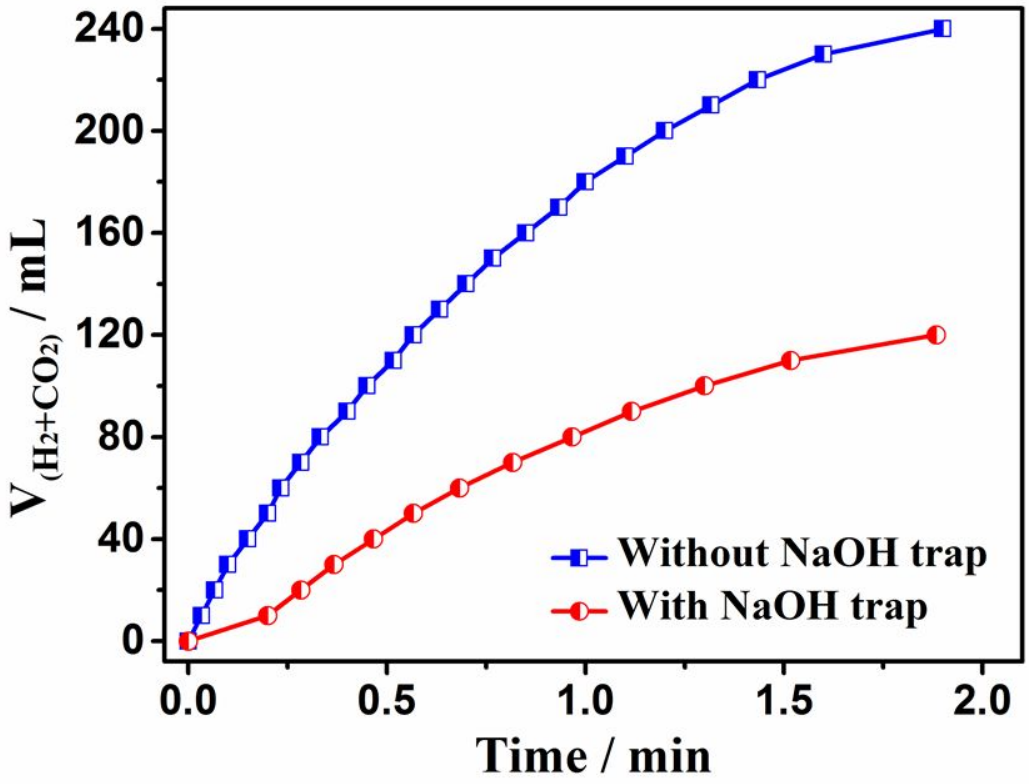

Figure S11. Volume of generated gas (H_2 + CO_2) versus time for the dehydrogenation of FA in FA-SF aqueous solution at 298 K over IrPdAu/NH_2-SBA-15 with/without 10 M NaOH trap (n_{FA}/n_{SF} = 1; n_{metal}/n_{FA} = 0.01).

NaOH trap experiments were performed to determine the volume ratio of H_2 to CO_2 in the gas generated during the IrPdAu/NH_2-SBA-15 catalyzed decomposition of FA. The generated gas was treated with/without NaOH trap (10 M NaOH aqueous solution), and its volume was monitored using the gas burette. As is shown in Figure S11, the volume of generated gas was reduced to half after treating with the NaOH trap, this result is indicative of the complete adsorption of CO_2 in NaOH solution (1) and the generated gas is H_2 and CO_2 with the volume ratio of 1:1, suggesting that the present IrPdAu/NH_2-SBA-15 has an 100% H_2 selectivity for the dehydrogenation of FA.

$$2NaOH + CO_2 \rightarrow Na_2CO_3 + H_2O \qquad (1)$$

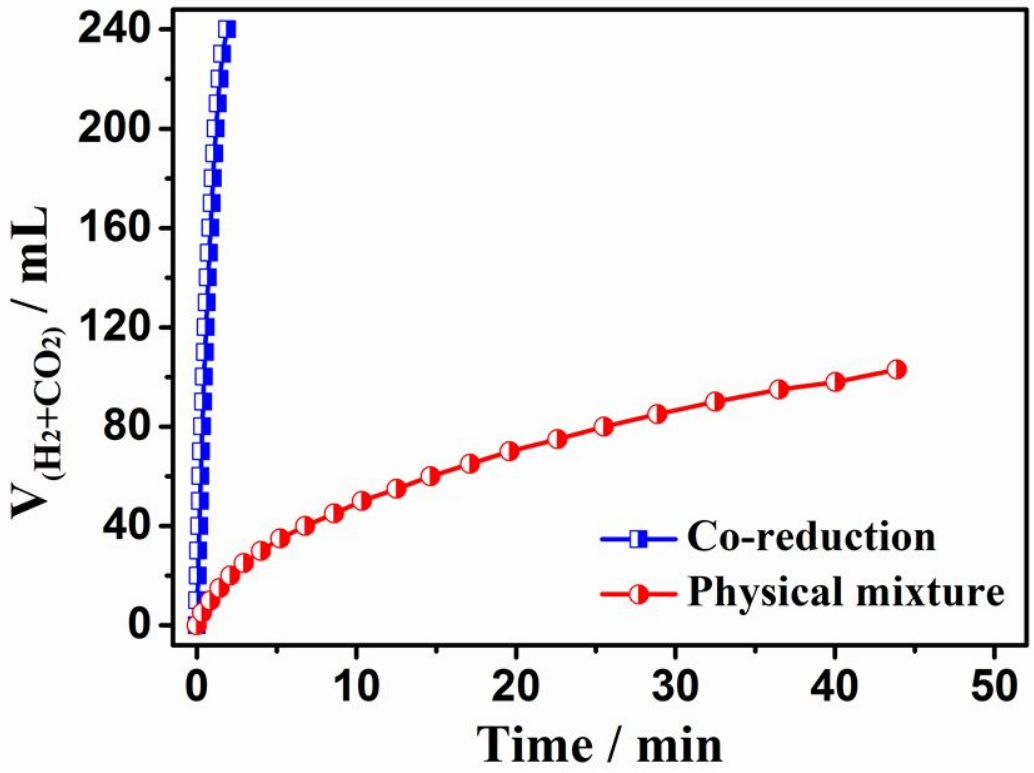

Figure S12. Volume of generated gas (H_2 + CO_2) versus time for the dehydrogenation of FA in FA-SF aqueous solution at 298 K over co-reduction prepared IrPdAu/NH_2-SBA-15 and the physical mixture of Ir/NH_2-SBA-15, Pd/NH_2-SBA-15, and Au/NH_2-SBA-15.

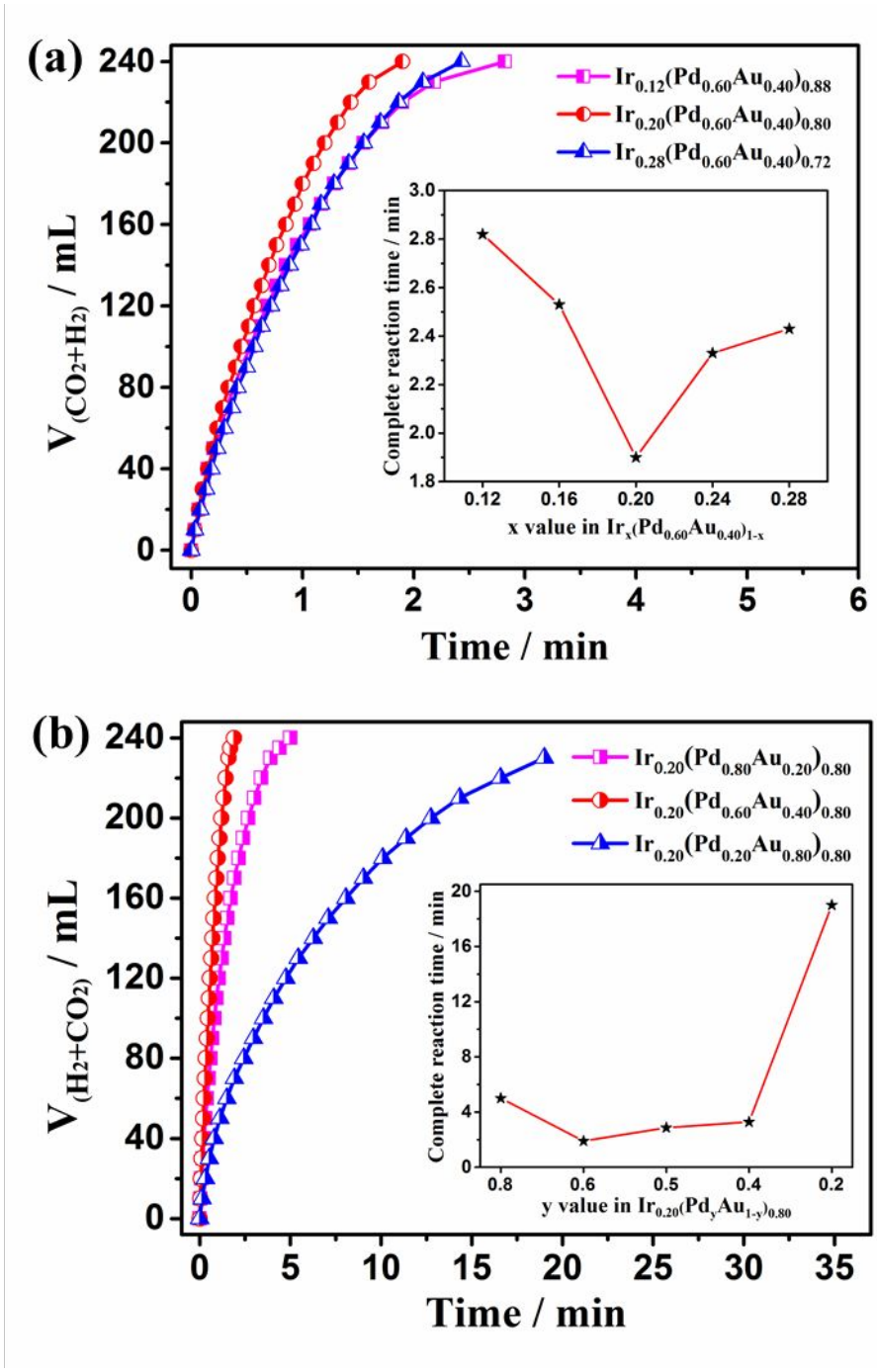

Figure S13. Volume of generated gas (H_2 + CO_2) versus time for the dehydrogenation of FA in FA-SF aqueous solution at 298 K in the presence of (a) $Ir_x(Pd_{0.6}Au_{0.4})_{1-x}/NH_2$-SBA-15 with different x values; (b) $Ir_{0.20}(Pd_yAu_{1-y})_{0.80}/NH_2$-SBA-15 with different y values; Inset: corresponding complete reaction time (n_{FA}/n_{SF} = 1; n_{metal}/n_{FA} = 0.01).

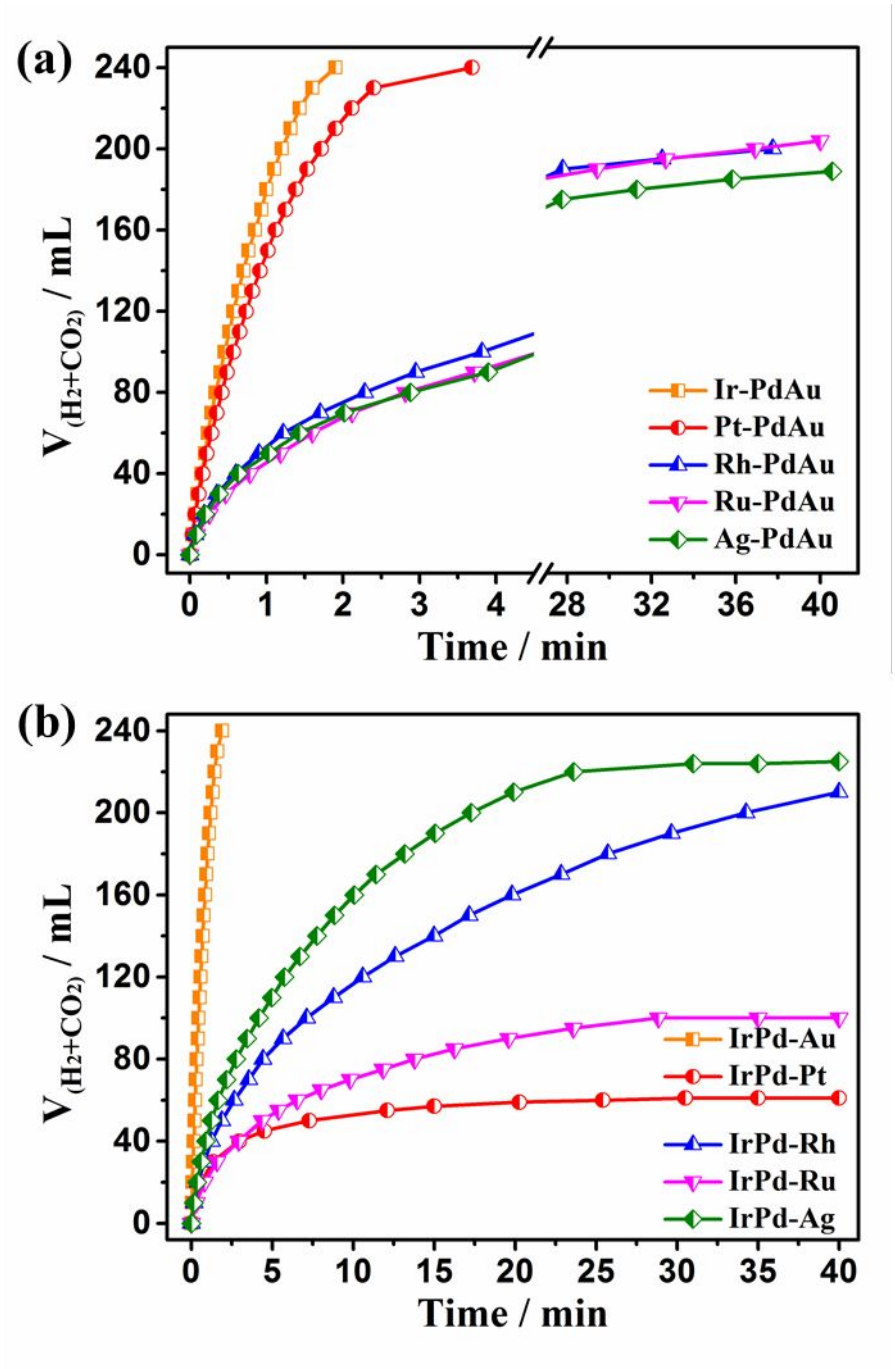

Figure S14. Volume of generated gas (H_2 + CO_2) versus time for the dehydrogenation of FA in FA-SF aqueous solution at 298 K over (a) M-PdAu/NH_2-SBA-15 (M= Ir, Pt, Rh, Ru, and Ag), (b) IrPd-N/NH_2-SBA-15 (N= Au, Pt, Rh, Ru, and Ag) (n_{FA}/n_{SF} = 1; n_{metal}/n_{FA} = 0.01).

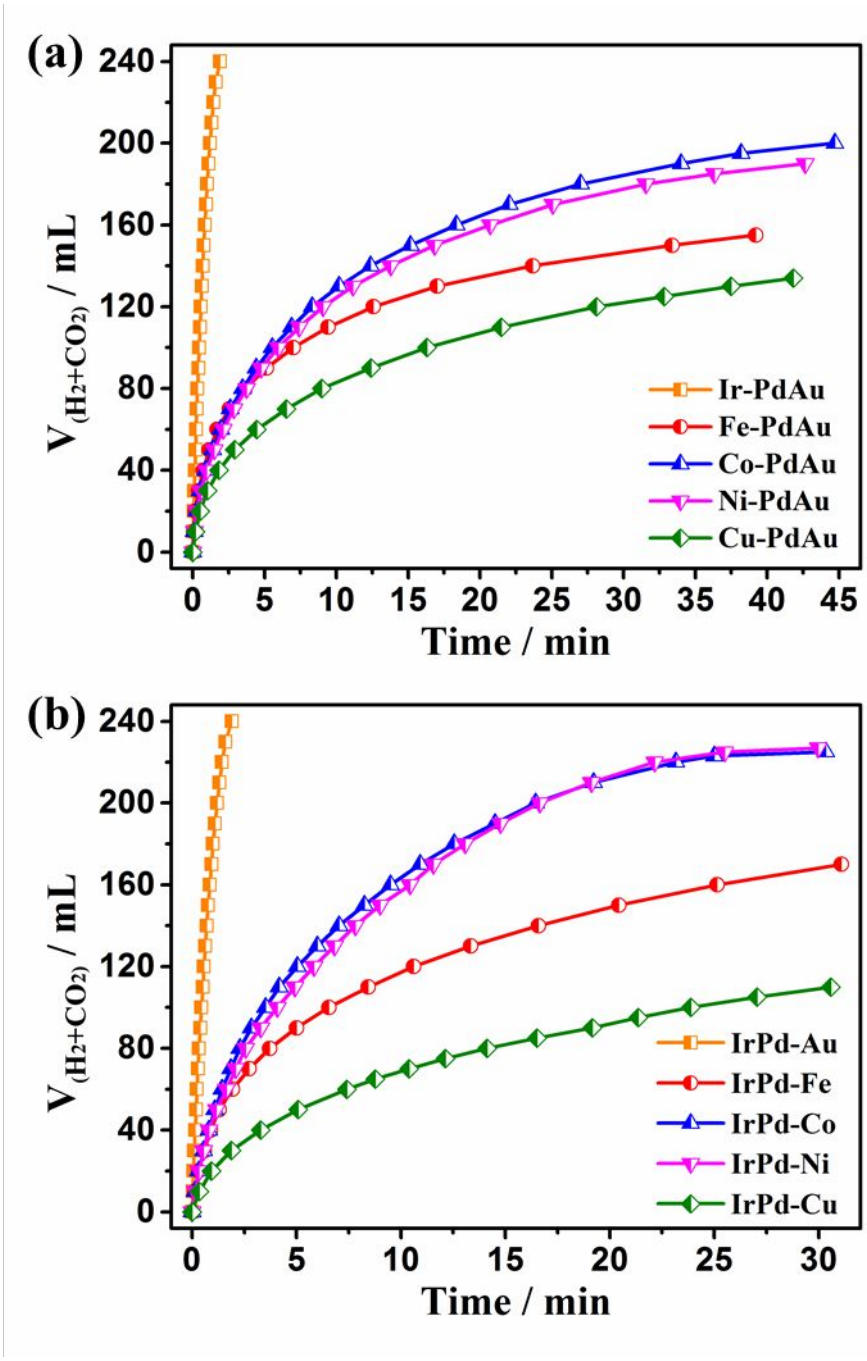

Figure S15. Volume of generated gas (H_2 + CO_2) versus time for the dehydrogenation of FA in FA-SF aqueous solution at 298 K over (a) P-PdAu/NH_2-SBA-15 (P= Ir, Fe, Co, Ni, and Cu) and (b) IrPd-Q/NH_2-SBA-15 (Q= Au, Fe, Co, Ni, and Cu) (n_{FA}/n_{SF} = 1; n_{metal}/n_{FA} = 0.01).

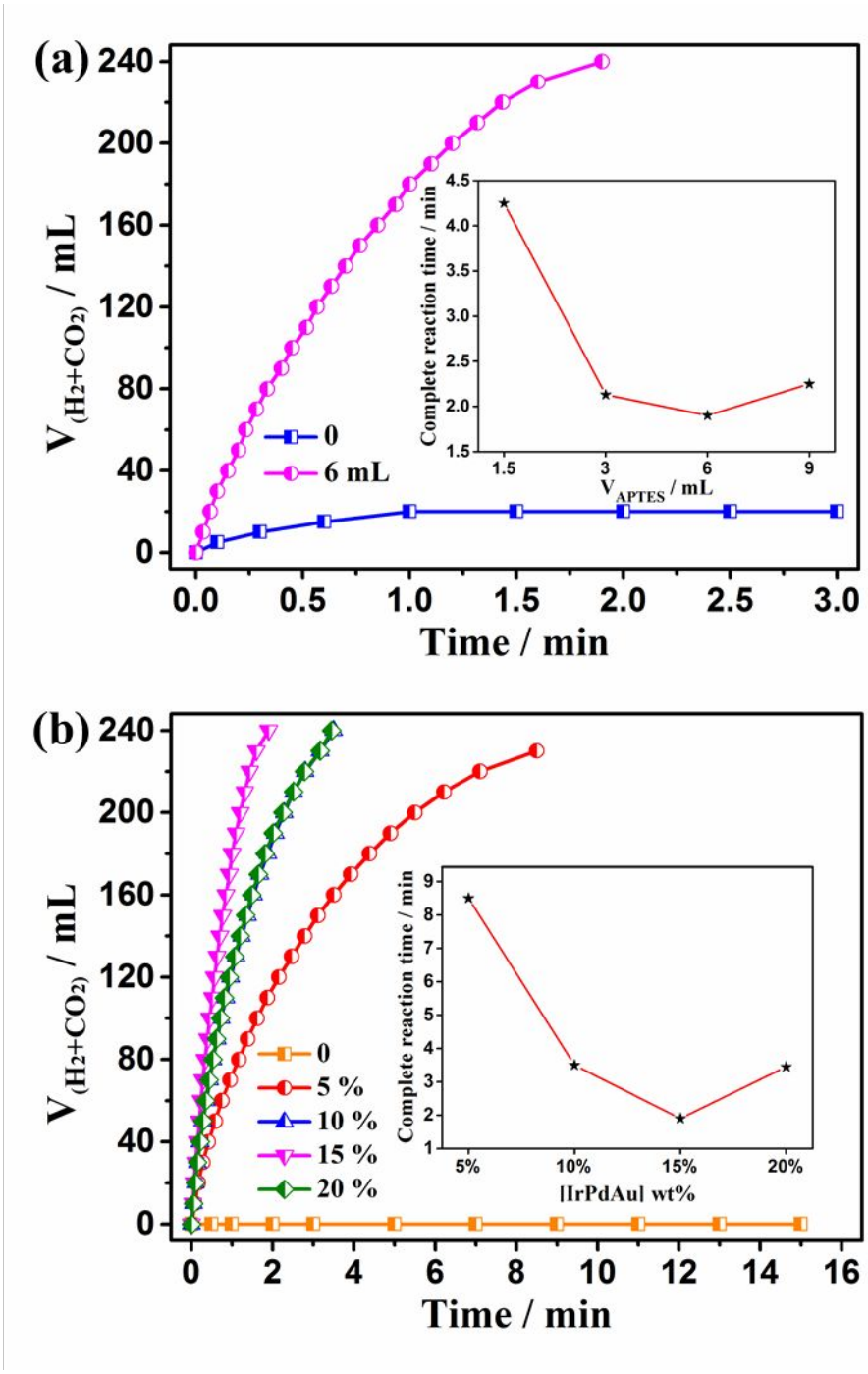

Figure S16. Volume of generated gas (H_2 + CO_2) versus time for the dehydrogenation of FA in FA-SF aqueous solution at 298 K over IrPdAu/NH_2-SBA-15 with (a) varying APTES dosage; (b) varying IrPdAu loading; (inset) corresponding complete reaction time (n_{FA}/n_{SF} = 1; n_{metal}/n_{FA} = 0.01).

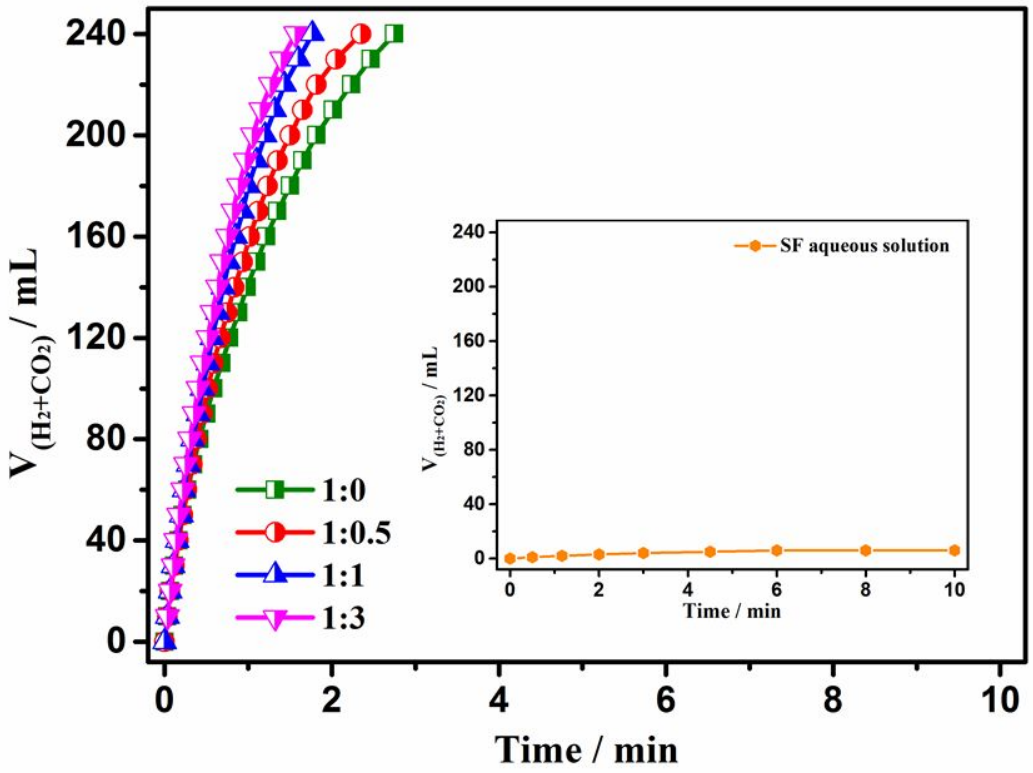

Figure S17. Volume of generated gas (H_2 + CO_2) versus time for the dehydrogenation of FA-SF aqueous solution at 298 K over IrPdAu/NH_2-SBA-15 in the presence of different mole ratio of FA/SF and (inset) pure SF aqueous solution (n_{metal}/n_{FA} = 0.01).

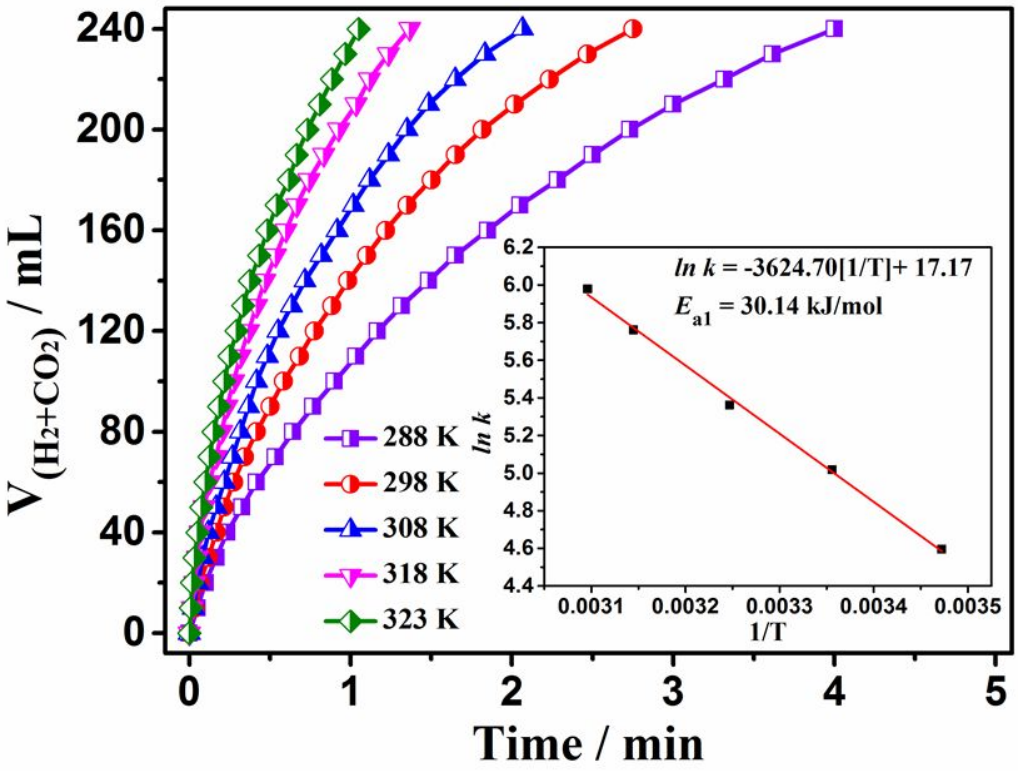

Figure S18. Volume of generated gas (H_2 + CO_2) versus time for the dehydrogenation of pure FA aqueous solution over IrPdAu/NH_2-SBA-15 at different temperature without the addition of SF. Inset: corresponding kinetic parameters (n_{metal}/n_{FA} = 0.01).

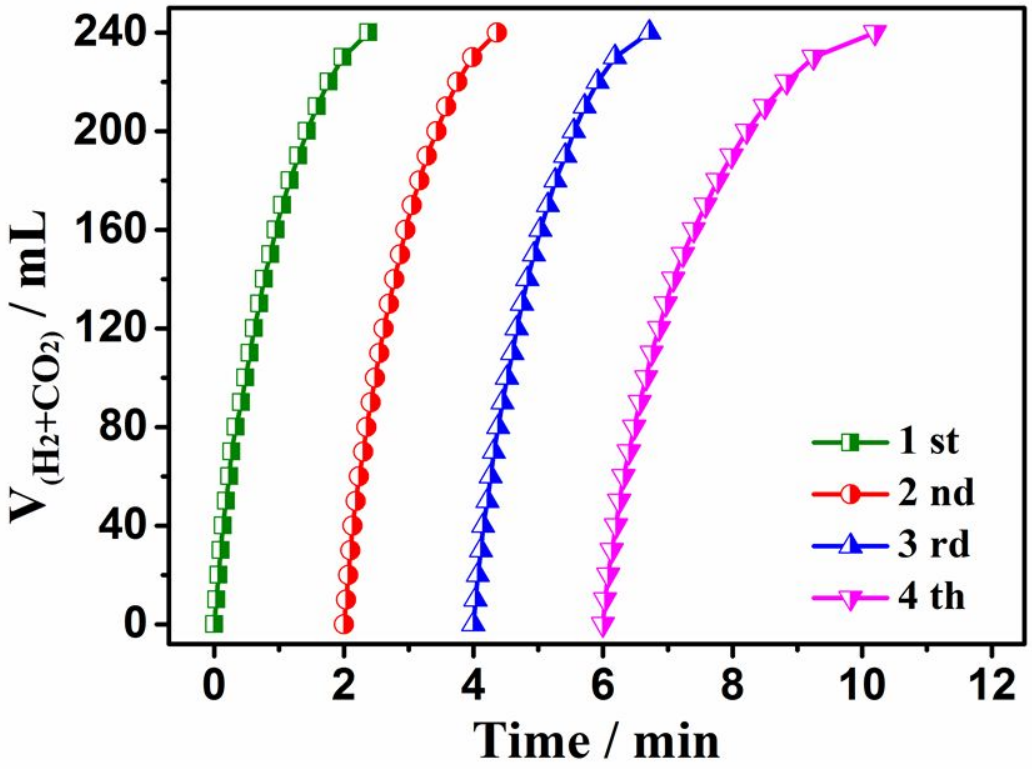

Figure S19. Reusability test of the optimized IrPdAu/NH_2-SBA-15 for the dehydrogenation of FA in FA-SF aqueous solution at 298 K.

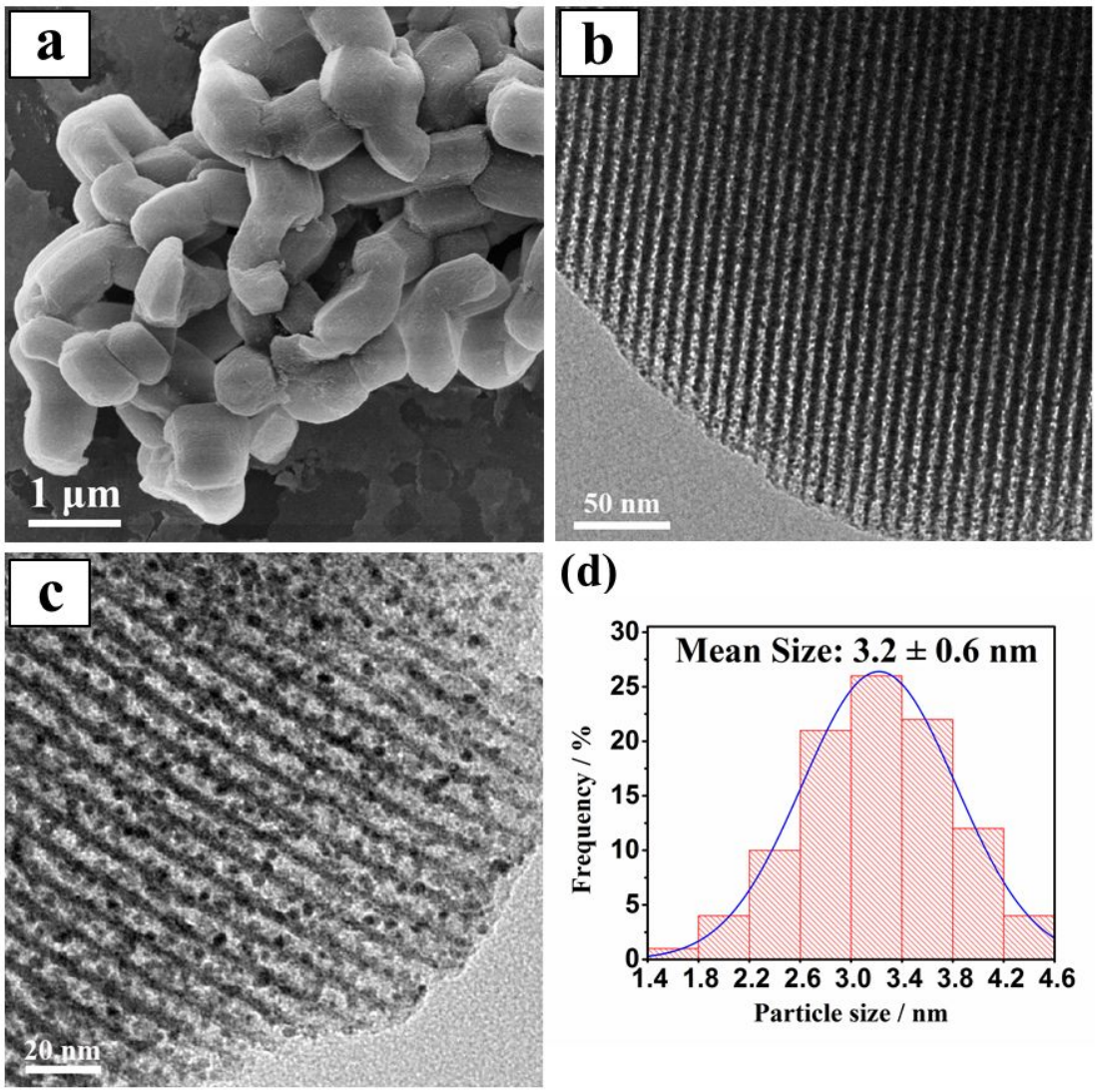

Figure S20. (a) SEM image, (b,c) TEM images, and (d) corresponding particle size distribution of IrPdAu/NH_2-SBA-15 after reusability test.

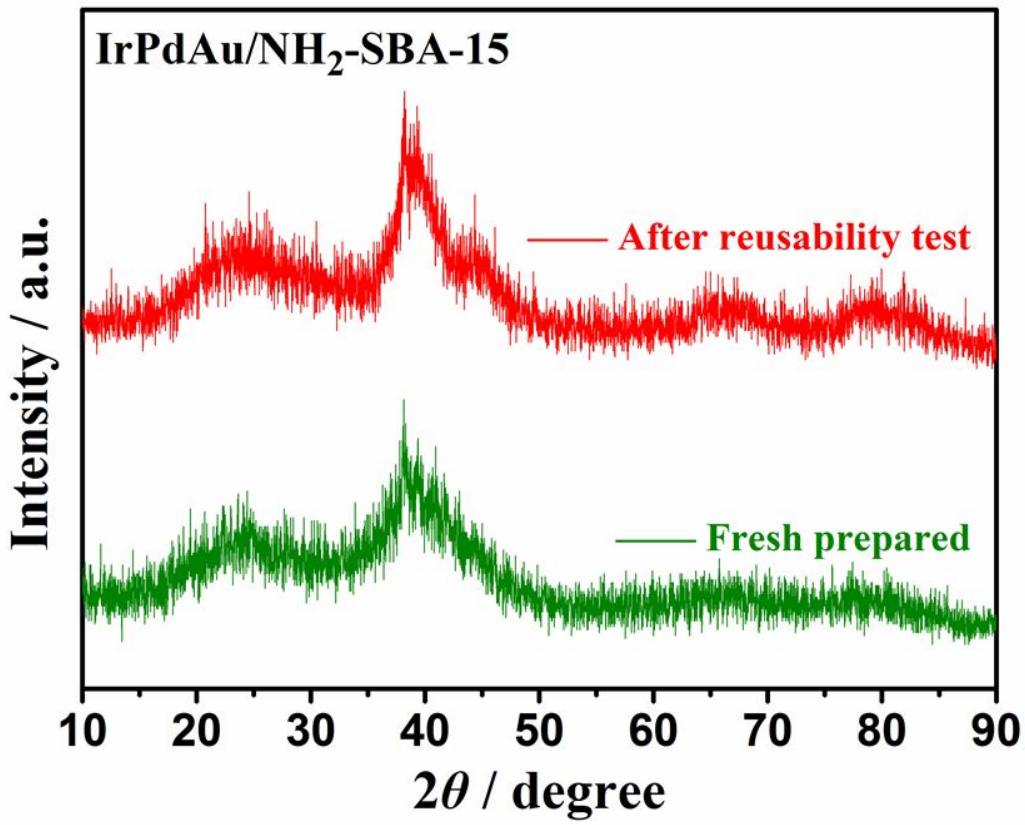

Figure S21. Wide-angle XRD pattern of IrPdAu/NH_2-SBA-15 before/after reusability test.

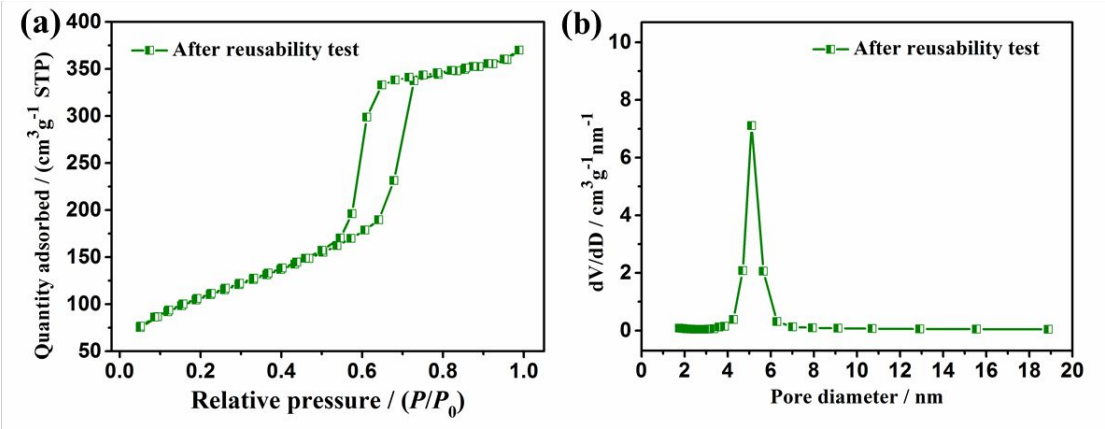

Figure S22. (a) Nitrogen adsorption-desorption isotherms and (b) corresponding pore diameter distribution curves of IrPdAu/NH_2-SBA-15 after reusability test.

Table S1 BET specific surface area, pore diameter, and pore volume of SBA-15, NH_2-SBA-15, and IrPdAu/NH_2-SBA-15 before/after dehydrogenation action.

No.	Sample	Specific surface area ($m^2\ g^{-1}$)	Pore volume ($cm^3\ g^{-1}$)	Pore size (nm)
1	SBA-15	673.19	0.94	5.66
2	NH_2-SBA-15	338.53	0.52	5.04
3	IrPdAu/NH_2-SBA-15 (Fresh prepared)	326.16	0.49	4.95
4	IrPdAu/NH_2-SBA-15 (After reusability test)	383.86	0.59	5.28

Table S2 ICP-OES (Ir, Pd, and Au) and elemental analyses (N, C, and H) for IrPdAu/NH_2-SBA-15 before/after dehydrogenation reaction.

Conditions	Ir (wt%)	Pd (wt%)	Au (wt%)	N (wt%)	C (wt%)	H (wt%)
Fresh prepared	3.50	5.05	6.38	1.98	5.92	1.98
After reusability test	3.63	5.08	6.39	1.57	4.73	1.85

Table S3 Catalytic activity for the dehydrogenation of formic acid catalyzed by different heterogeneous catalysts.

Catalysts	Temp. (K)	Additive	Ea (kJ/mol)	TOF[a] (h^{-1})	Ref.
Without Additive					
IrPdAu/NH_2-SBA-15	298	None	30.1	4737	This work
$Au_{0.5}Pd_{0.5}$/NH_2-N-rGO	298	None	--	4445.6	S8
$Ag_{0.025}Pd_{0.975}$/NH_2-N-rGO	298	None	--	2556.2	S8
Pd_1Au_1/30-LA	298	None	38.9	1881[b]	S9
AP-SiO_2@PDA-NGO@Pd	298	None	51.5	1588[b]	S10
PdAu-MnO_x/N-SiO_2	298	None	26.2	785	S11
CrAuPd/N-SiO_2	298	None	49.8	730	S12
AuPd-MnO_x/ZIF-8-rGO	298	None	--	382.1	S13
Au@Pd/N-mrGO	298	None	--	89.1	S14
$Co_{0.30}Au_{0.35}Pd_{0.35}$/C	298	None	--	80	S15
$Ag_{0.2}Au_{0.4}Pd_{0.4}$/rGO	298	None	--	73.6	S16
Au@Schiff-SiO_2	323	None	71.6	4368	S17
With Additive					
IrPdAu/NH_2-SBA-15	298	SF	31.4	6316	This work
Pd@CN900K	298	SF	46.9	1963[b]	S18
Au_2Pd_3@(P)N-C	303	SF	34.8	5400[b]	S19
Pd_1Au_1/72-LA	303	SF	34.4	3583[b]	S9
In situ-Pd@MSC	303	SF	31.7	2965	S20
Pd@SS-CNR	303	SF	38.8	1878[b]	S21
$(Co_6)Ag_{0.1}Pd_{0.9}$/RGO	323	SF	43.1	2739[b]	S22
Au/ZrO_2 NCs	323	NEt_3	49.3	1593	S23
$Pd_{0.6}Ag_{0.4}$@ZrO_2/C/rGO	333	SF	50.1	4500	S24
AuPd@ED-MIL-101	363	SF	--	106	S25
PdAu@Au/C	365	SF	--	59.6	S26

[a] Initial TOF values calculated on initial reaction time or initial conversion of FA.

[b] TOF values calculated on the complete time of gas releasing.

Reference

[S1]Zhao, D.; Huo, Q.; Feng, J.; Chmelka, B. F.; Stucky, G. D. Nonionic Triblock and Star Diblock Copolymer and Oligomeric Surfactant Syntheses of Highly Ordered, Hydrothermally Stable, Mesoporous Silica Structures. *J. Am. Chem. Soc.* **1998**, *120*, 6024-6036.

[S2]Koh, K.; Seo, J.-E.; Lee, J. H.; Goswami, A.; Yoon, C. W.; Asefa, T. Ultrasmall Palladium Nanoparticles Supported on Amine-Functionalized SBA-15 Efficiently Catalyze Hydrogen Evolution from Formic Acid. *J. Mater. Chem. A* **2014**, *2*, 20444-20449.

[S3]Chatterjee, S.; Paital, A. R. Functionalized Cubic Mesoporous Silica as a Non-Chemodosimetric Fluorescence Probe and Adsorbent for Selective Detection and Removal of Bisulfite Anions along with Toxic Metal Ions. *Adv. Funct. Mater.* **2017,** 1704726.

[S4]Miao, W.; Zhang, C.; Cai, Y.; Zhang, Y.; Lu, H. Fast Solid-Phase Extraction of N-Linked Glycopeptides by Amine-Functionalized Mesoporous Silica Nanoparticles. *Analyst* **2016**, *141*, 2435-2440.

[S5]Zhao, L.; Sui, D.; Wang, Y. Fluorescence Chemosensors Based on Functionalized SBA-15 for Detection of Pb^{2+} in Aqueous Media. *RSC Adv.* **2015**, *5*, 16611-16617.

[S6]Zhang, Z.; Cheng, J.; Luo, Y.; Shi, W.; Wang, W.; Zhang, B.; Zhang, R.; Bao, X.; Guo, Y.; Cui, F. Pt Nanoparticles Supported on Amino-Functionalized SBA-15 for Enhanced Aqueous Bromate Catalytic Reduction. *Catal. Commun.* **2018**, *105*,

11-15.

[S7]Ma, Q.; Wang, N.; Liu, G.; Wang, L. Enhanced Performance of Pd Nanoparticles on SBA-15 Grafted with Alkyltrialkoxysilane in 2-Ethyl-Anthraquinone Hydrogenation. *Microporous Mesoporous Mater.* **2019**, *279*, 245-251.

[S8]Li, S.-J.; Zhou, Y.-T.; Kang, X.; Liu, D.-X.; Gu, L.; Zhang, Q.-H.; Yan, J.-M.; Jiang, Q. A Simple and Effective Principle for a Rational Design of Heterogeneous Catalysts for Dehydrogenation of Formic Acid. *Adv. Mater.* **2019**, 1806781.

[S9]Hong, W.; Kitta, M.; Tsumori, N.; Himeda, Y.; Autrey, T.; Xu, Q. Immobilization of Highly Active Bimetallic PdAu Nanoparticles onto Nanocarbons for Dehydrogenation of Formic Acid. *J. Mater. Chem. A* **2019**, *7*, 18835-18839.

[S10]Ye, W.; Pei, W.; Zhou, S.; Huang, H.; Li, Q.; Zhao, J.; Lu, R.; Ge, Y.; Zhang, S. Controlling the Synthesis of Uniform Electron-Deficient Pd Clusters for Superior Hydrogen Production from Formic Acid. *J. Mater. Chem. A* **2019**, *7*, 10363-10371.

[S11]Karatas, Y.; Bulut, A.; Yurderi, M.; Ertas, I. E.; Alal, O.; Gulcan, M.; Celebi, M.; Kivrak, H.; Kaya, M.; Zahmakiran, M. PdAu-MnO_x Nanoparticles Supported on Amine-Functionalized SiO_2 for the Room Temperature Dehydrogenation of Formic Acid in the Absence of Additives. *Appl. Catal., B* **2016**, *180*, 586-595.

[S12]Yurderi, M.; Bulut, A.; Caner, N.; Celebi, M.; Kaya, M.; Zahmakiran, M. Amine

Grafted Silica Supported CrAuPd Alloy Nanoparticles: Superb Heterogeneous Catalysts for the Room Temperature Dehydrogenation of Formic Acid. *Chem. Commun.* **2015**, *51*, 11417-11420.

[S13]Yan, J.-M.; Wang, Z.-L.; Gu, L.; Li, S.-J.; Wang, H.-L.; Zheng, W.-T.; Jiang, Q. AuPd-MnO_x/MOF-Graphene: An Efficient Catalyst for Hydrogen Production from Formic Acid at Room Temperature. *Adv. Energy Mater.* **2015**, 1500107.

[S14]Wang, Z.-L.; Yan, J.-M.; Wang, H.-L.; Ping, Y.; Jiang, Q. Au@Pd Core-Shell Nanoclusters Growing on Nitrogen-Doped Mildly Reduced Graphene Oxide with Enhanced Catalytic Performance for Hydrogen Generation from Formic Acid. *J. Mater. Chem. A* **2013,** *1*, 12721-12725.

[S15]Wang, Z.-L.; Yan, J.-M.; Ping, Y.; Wang, H.-L.; Zheng, W.-T.; Jiang, Q. An Efficient CoAuPd/C Catalyst for Hydrogen Generation from Formic Acid at Room Temperature. *Angew. Chem. Int. Ed.* **2013**, *52*, 4406-4409.

[S16]Li, S.-J.; Ping, Y.; Yan, J.-M.; Wang, H.-L.; Wu, M.; Jiang, Q. Facile Synthesis of AgAuPd/Graphene with High Performance for Hydrogen Generation from Formic Acid. *J. Mater. Chem. A* **2015**, *3*, 14535-14538.

[S17]Liu, Q.; Yang, X.; Huang, Y.; Xu, S.; Su, X.; Pan, X.; Xu, J.; Wang, A.; Liang, C.; Wang, X.; Zhang, T. A Schiff Base Modified Gold Catalyst for Green and Efficient H_2 Production from Formic Acid. *Energy Environ. Sci.* **2015**, *8*, 3204-3207.

[S18]Wang, Q.; Tsumori, N.; Kitta, M.; Xu, Q. Fast Dehydrogenation of Formic Acid over Palladium Nanoparticles Immobilized in Nitrogen-Doped Hierarchically

Porous Carbon. *ACS Catal.* **2018**, *8*, 12041-12045.

[S19]Wang, Q.; Chen, L.; Liu, Z.; Tsumori, N.; Kitta, M.; Xu, Q. Phosphate-Mediated Immobilization of High-Performance AuPd Nanoparticles for Dehydrogenation of Formic Acid at Room Temperature. *Adv. Funct. Mater.* **2019**, 1903341.

[S20]Zhu, Q.-L.; Song, F.-Z.; Wang, Q.-J.; Tsumori, N.; Himeda, Y.; Autrey, T.; Xu, Q. A Solvent-Switched in Situ Confinement Approach for Immobilizing Highly-Active Ultrafine Palladium Nanoparticles: Boosting Catalytic Hydrogen Evolution. *J. Mater. Chem. A* **2018**, *6*, 5544-5549.

[S21]Zou, L.; Kitta, M.; Hong, J.; Suenaga, K.; Tsumori, N.; Liu, Z.; Xu, Q. Fabrication of a Spherical Superstructure of Carbon Nanorods. *Adv. Mater.* **2019**, 1900440.

[S22]Chen, Y.; Zhu, Q.-L.; Tsumori, N.; Xu, Q. Immobilizing Highly Catalytically Active Noble Metal Nanoparticles on Reduced Graphene Oxide: A Non-Noble Metal Sacrificial Approach. *J. Am. Chem. Soc.* **2015**, *137*, 106-109.

[S23]Bi, Q.-Y.; Du, X.-L.; Liu, Y.-M.; Cao, Y.; He, H.-Y.; Fan, K.-N. Efficient Subnanometric Gold-Catalyzed Hydrogen Generation via Formic Acid Decomposition under Ambient Conditions. *J. Am. Chem. Soc.* **2012**, *134*, 8926-8933.

[S24]Song, F.-Z.; Zhu, Q.-L.; Yang, X.; Zhan, W.-W.; Pachfule, P.; Tsumori, N.; Xu, Q. Metal-Organic Framework Templated Porous Carbon-Metal Oxide/Reduced Graphene Oxide as Superior Support of Bimetallic Nanoparticles for Efficient Hydrogen Generation from Formic Acid. *Adv. Energy Mater.* **2018**, *8*, 1701416.

[S25]Gu, X.; Lu, Z.-H.; Jiang, H.-L.; Akita, T.; Xu, Q. Synergistic Catalysis of Metal-Organic Framework-Immobilized Au-Pd Nanoparticles in Dehydrogenation of Formic Acid for Chemical Hydrogen Storage. *J. Am. Chem. Soc.* **2011**, *133*, 11822-11825.

[S26]Huang, Y.; Zhou, X.; Yin, M.; Liu, C.; Xing, W. Novel PdAu@Au/C Core-Shell Catalyst: Superior Activity and Selectivity in Formic Acid Decomposition for Hydrogen Generation. *Chem. Mater.* **2010**, *22*, 5122-5128.